Available online at www.sciencedirect.com
ScienceDirect
Journal of the European Ceramic Society 29 (2009) 2969–2978
www.elsevier.com/locate/jeurceramsoc

Mg-substituted hydroxyapatite nanopowders: Synthesis, thermal stability and sintering behaviour

Ilaria Cacciotti [a,*], Alessandra Bianco [a], Mariangela Lombardi [b], Laura Montanaro [b]

[a] *University of Rome "Tor Vergata", Department of Chemical Science and Technology, INSTM RU Tor Vergata, Via della Ricerca Scientifica, Rome, Italy*
[b] *Politecnico di Torino, Department of Material Science and Chemical Engineering, INSTM RU Politecnico di Torino, LINCE Lab Torino, Italy*

Received 21 January 2009; received in revised form 27 April 2009; accepted 30 April 2009
Available online 3 June 2009

Abstract

This paper reports a systematic investigation on Mg-substituted hydroxyapatite ($Ca_{10-x}Mg_x(PO_4)_6(OH)_2$) nanopowders produced by precipitation of $Ca(NO_3)_2{\cdot}4H_2O$ and $Mg(NO_3)_2$. The Mg content ranged between 0.6 and 2.4 wt%. Semicrystalline Mg-substituted hydroxyapatite powders made up of needle-like nanoparticles were obtained, the specific surface area ranged between 87 and 142 m^2/g. Pure hydroxyapatite nanopowder decomposed around 1000 °C. Mg-substituted hydroxyapatites were thermally stable up to 660 °C ($x = 1.0$), 760 °C ($x = 0.5$) and 840 °C ($x = 0.25$) showing a distinct decreased thermal stability with respect to the pure sample.

A relevant displacement of the sintering curve at lower temperature as a function of Mg content was observed, comparing to the behaviour of a pure HAp material, synthesized following the same procedure, and ascribed to the β-TCP formation.

Keywords: A. Powders-chemical preparation; B. Microstructure; C. Thermal properties; D. Apatite; E. Biomedical applications

1. Introduction

Hydroxyapatite (HAp, $Ca_{10}(PO_4)_6(OH)_2$) and β-tricalcium phosphate (β-TCP, *whitlockite,* β-$Ca_3(PO_4)_2$) are the most used calcium phosphate compounds as bone grafting materials in hard tissue implants and as materials for bone–tissue engineering applications, due to their excellent biocompatibility, ability to promote cellular functions and expressions, and osteoconductivity.[1] The HAp lattice easily incorporates a variety of substituents in the apatite structure, inducing modifications in powder crystallinity, particle morphology, lattice parameters and thermal stability. It is well known that trace quantities of cations (i.e. Mg^{2+}, Zn^{2+}, Sr^{2+}) and/or anions (i.e. $SiO_4{}^{4-}$, F^-, $CO_3{}^{2-}$) in HAp play a pivotal role in its overall biological performances. Among substituting cations, magnesium is widely studied, being the fourth most abundant cation in the human body (0.44–1.23 wt%). Enamel, dentin and bone contain, respectively, 0.44, 1.23, and 0.72 wt% of Mg.[2] It is well known that magnesium is closely associated with the mineralization of calcified tissues, directly stimulating osteoblast proliferation.[3,4] Magnesium depletion adversely affects all stages of skeletal metabolism, causing cessation of bone growth, decreased osteoblastic and osteoclastic activities, osteopenia and bone fragility.[5] Consequently, the incorporation of Mg ions into the HAp lattice is of great interest for the developing of artificial bones. It has been shown that the presence of Mg^{2+} within HAp lattice sensibly affects apatite crystallization in solution and its thermal stability, promoting the formation of β-TCP and thus forming biphasic calcium phosphates (BCP). Besides, the incorporation of Mg^{2+} stabilizes the β-TCP phase, increasing its transition temperature to α-TCP above 1125 °C.

These materials are considered promising substitutes for bone replacement due to their unique biological features.[6] In addition, the control of Mg^{2+} incorporation results in tailored crystallinity, solubility and morphology of the synthesized nanocrystals.[4]

The objective of this work is to synthesise pure and Mg-substituted hydroxyapatite nanostructured powders with different Mg contents, aimed to study their sintering behaviour. In fact, on our knowledge, only few papers report a systematic study focused on this relevant topic. Particle size and morphology were studied by electron microscopy (TEM, SEM), composition was determined by induced coupled plasma–atomic emission spectroscopy and specific surface area by N_2 adsorption isotherms. Characteristic functional groups

* Corresponding author. Tel.: +39 0672594482; fax: +39 0672594328.
E-mail address: ilaria.cacciotti@uniroma2.it (I. Cacciotti).

0955-2219/$ – see front matter © 2009 Elsevier Ltd. All rights reserved.
doi:10.1016/j.jeurceramsoc.2009.04.038

Table 1
Designation and nominal composition of pure and Mg-substituted hydroxyapatites.

Sample	Formula	Ca/P molar ratio	(Ca + Mg)/P molar ratio
HAp	$Ca_{10}(PO_4)_6(OH)_2$	1.667	–
0.25Mg-HAp (0.60 wt%)	$Ca_{9.75}Mg_{0.25}(PO_4)_6(OH)_2$	1.625	1.667
0.5Mg-HAp (1.2 wt%)	$Ca_{9.5}Mg_{0.5}(PO_4)_6(OH)_2$	1.583	1.667
1.0Mg-HAp (2.4 wt%)	$Ca_9Mg(PO_4)_6(OH)_2$	1.500	1.667

were evidenced by Fourier transform infrared spectroscopy (FT-IR), the thermal behaviour followed by thermal analysis (DTA), thermal stability evaluated by X-ray diffractometry (XRD, HT-XRD). Crystallinity degree, average crystallite size and cell parameters were also estimated. The sintering behaviour was evaluated by thermal dilatometry. Density and microstructure of sintered ceramics are also presented and discussed.

2. Experimental

2.1. Synthesis of pure and Mg-substituted hydroxyapatite

Pure and Mg-substituted hydroxyapatite powders were synthesised in a double-walled jacket reactor at 40 °C under magnetic stirring starting from calcium nitrate and diammonium hydrogen phosphate.

Pure hydroxyapatite powder (HAp) was prepared adding drop-wise (3–4 drops/s) 250 ml of an 1 M aqueous solution of calcium nitrate tetrahydrate ($Ca(NO_3)_2{\cdot}4H_2O$, *Aldrich* 99.2%, MW 236.15) to a diammonium hydrogen phosphate ($(NH_4)_2HPO_4$, *Aldrich* 99.2%, MW 132.06) solution, by the following reaction:

$$10Ca(NO_3)_2{\cdot}4H_2O + 6(NH_4)_2HPO_4 + 2NH_4OH \rightarrow Ca_{10}(PO_4)_6(OH)_2 + 20NH_4NO_3 + 46H_2O$$

The pH was continuously monitored and adjusted to 10 ± 0.1 by adding NH_4OH conc. More details have been published elsewhere.[7]

Magnesium-substituted hydroxyapatite powders (Mg-HAp) of different composition ($Ca_{10-x}Mg_x(PO_4)_6(OH)_2$, $0.25 \leq x \leq 1.0$) were prepared assuming that magnesium ions would substitute for the calcium site in the HAp lattice in order to obtain a nominal composition in term of (Ca + Mg)/P ratio of 1.667 (Table 1). Mg-HAp powders were synthesised, adding magnesium nitrate hexahydrate ($Mg(NO_3)_2{\cdot}6H_2O$, *Carlo Erba 101.5%*, MW 256.41) to calcium nitrate tetrahydrate solution, in different concentrations (i.e. 0.025, 0.05, 0.1 M). Then, the same procedure described above was followed. The following reaction occurred:

$$(10-x)Ca(NO_3)_2{\cdot}4H_2O + xMg(NO_3)_2{\cdot}6H_2O + 6(NH_4)_2HPO_4 + 2NH_4OH \rightarrow Ca_{10-x}Mg_x(PO_4)_6(OH)_2 + 20NH_4NO_3 + (6 + 4(10-x) + 6x)H_2O \qquad 0.25 \leq x \leq 1$$

All precipitates were aged in mother liquor at room temperature for 24 h, washed with an aqueous NH_4OH solution, vacuum filtered, and finally dried in oven at 60 °C (as-dried samples).

Sample designation, nominal compositions and formula of all synthesised materials are summarised in Table 1.

2.2. Characterisation techniques

Chemical analyses of precipitates were performed by Induced Coupled Plasma Atomic Emission Spectroscopy (*AES-ICP, JobinYvon JV 24R*). The detection limits of ICP analysis are 0.2 ppb at 393.366 nm for Ca, 76 ppb at 214.914 nm for P, and 1 ppb at 279.553 nm for Mg.

The thermal behaviour of as-dried samples was investigated by simultaneous thermogravimetry and differential thermal analysis (*TG–DTA, Netzsch STA 409*) in the following conditions: sample weight about 150 mg, heating rate 10 °C/min and peak temperature 1500 °C.

Microstructural features of as-dried powders were studied by Transmission Electron Microscopy (*TEM, Philips CM120*) in bright field mode, the accelerating voltage being 100 kV.

Infrared spectra (*Fourier Transform Infrared Spectroscopy, FTIR Perkin Elmer*) were recorder in the region 500–4000 cm^{-1} using KBr pellets (1%wt/wt), spectral resolution of 4 cm^{-1}.

The specific surface area (SSA) of as-dried samples and powders heated at 600 °C was evaluated by N_2 adsorption (*Sorptomatic 1900, Carlo Erba Instruments*) using Brunauer–Emmett–Teller (BET) method. The specific surface area was calculated from the volume of gas adsorbed in a monolayer.[8,9]

The particle size (D_{BET}) was also estimated by assuming the primary particles to be spherical

$$D_{BET} = \frac{6}{\rho \cdot s},$$

where ρ is the theoretical density of the sample (3.156 g/cm^3 for HAp and Mg-HAp) and s is the SSA.[10]

X-ray diffraction (XRD) (*Philips X'Pert 1710*) (Cu Kα radiation λ = 1.5405600 Å, 20–55° 2θ, step size 0.010°, time per step 2 s, scan speed 0.005°/s) analyses were performed on both as-dried and calcined powders at different temperatures up to 1500 °C for 2 h. Phase evolution of as-dried powders was followed by high temperature XRD measurements (HT-XRD) (*Anton Paar HTK 1200*) in the following conditions: Cu Kα radiation λ = 1.5405600 Å, 20–55° 2θ, heating rate 5 °C/min, peak temperature 1100 °C, step size 0.010°, time per step 2 s, scan speed 0.005°/s.

According to Landi et al.[11] the crystallinity degree of as-dried samples (X_c) corresponding to the fraction of crystalline

phase present in the examined volume was evaluated by the relation:

$$X_c \approx 1 - \frac{V_{112/300}}{I_{300}}$$

where I_{300} is the intensity of (3 0 0) reflection of HAp and $V_{112/300}$ is the intensity of the hollow between (1 1 2) and (3 0 0) reflections, which completely disappears in non-crystalline samples. In agreement with Landi et al. a verification was done with the relation:

$$B_{002}\sqrt[3]{X_c} = K$$

where K is a constant found equal to 0.24 for a very large number of different HAp powders, and B_{002} is the full-width at half-maximum (in degrees) of reflection (0 0 2).

The average crystallite size $D_{(hkl)}$ in nm was estimated following Debey–Scherrer equation[12]:

$$D_{()} = \frac{K\lambda}{\beta_{1/2}\cos\vartheta}$$

where K is the shape factor equal to 0.9, λ the X-ray wavelength (equal to 1.541 Å for Cu Kα radiation), θ the Bragg's diffraction angle (in degrees), $\beta_{1/2}$ the full-width at half-maximum (FWHM). The diffraction peak at 25.8° (2θ) corresponding to (0 0 2) Miller plane family of HAp (JCPDS file #09-0432) and the diffraction peak at 32.9° (2θ) were chosen to calculate the average crystal size along to the crystallographic axis c and a, respectively.[13,14]

Cell parameters of the hydroxyapatite phase were estimated through the *TREOR* algorithm (Philips X'Pert Plus software) for both pure and Mg-substituted powders, using XRD diffraction patterns of samples calcined at 1100 °C. The reference for HAp was JCPDS #09-0432 ($a = b = 9.418$ Å, $c = 6.884$ Å, space group P63/m, theoretical density 3.156 g/cm^3, $Z = 1$). The quantitative analyses in terms of volume fraction of β-TCP (X_β) were performed on powders calcined at 1100 °C as follows[15]:

$$W_\beta = \frac{I_{\beta(0210)}}{I_{\beta(0210)} + I_{H(211)}} \qquad X_\beta = \frac{PW_\beta}{1 + (P-1)W_\beta}$$

where $I_{\beta(0210)}$ and $I_{H(211)}$ are the XRD integrated intensity values of (0210) β-TCP and (211) HAp reflections. The coefficient P, representing the integrated intensity ratio of (211) HAp reflection to (0210) β-TCP reflection, was 2.275.[16]

Table 2
ICP-AES analysis of as-dried powders.

Sample	Ca/P molar ratio	Mg [mg/L]	(Ca + Mg)/P molar ratio
HAp	1.658	–	–
0.25Mg-HAp	1.683	0.48	1.686
0.5Mg-HAp	1.609	7.22	1.689
1.0Mg-HAp	1.505	1.86	1.518

2.3. Sintering behaviour of pure and Mg-substituted hydroxyapatite

On the grounds of TG–DTA and XRD analyses, powders were pre-treated at 600 °C for 1 h (heating and cooling rate of 10 °C/min) to prevent relevant weight losses during the densification process. Bars were cold uniaxially pressed at 400 MPa and dilatometric analyses (*Netzsch 402E*) were performed in the following conditions: peak temperature 1250 °C, soaking time 1 h, heating and cooling rate 10 °C/min. Green and final densities were evaluated by geometrical and mass measurements. Final microstructures were observed on fracture surfaces

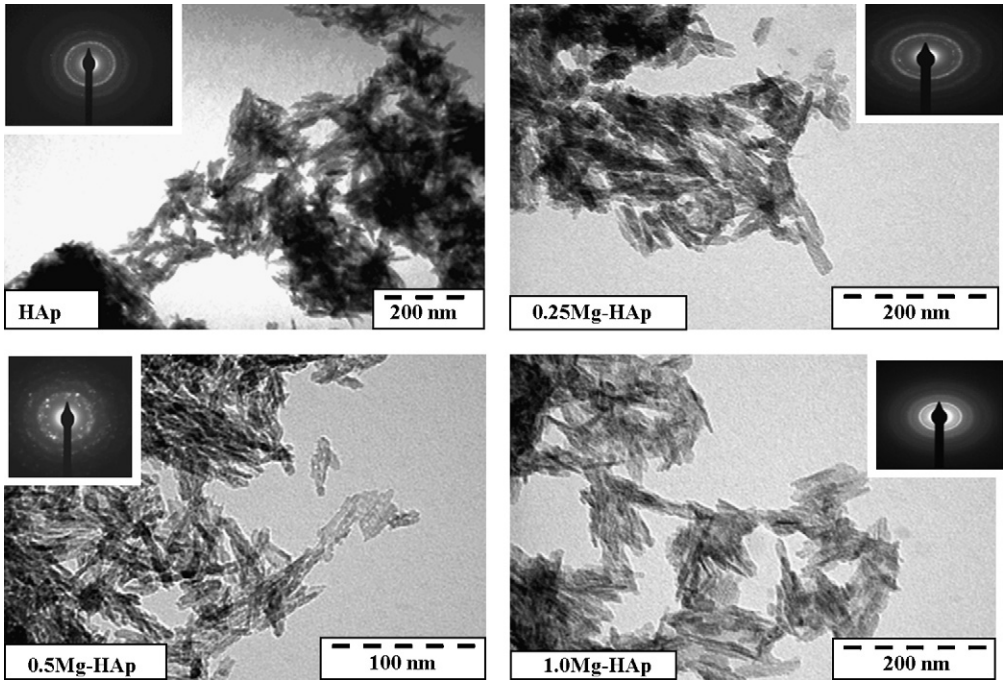

Fig. 1. TEM images and SAED patterns of as-dried samples of pure and Mg-substituted hydroxyapatite.

by the mean of a scanning electron microscope (*SEM, Hitachi S2300*).

3. Results and discussion

3.1. Microstructure and thermogravimetry of as-dried precipitates

ICP-AES results on as-dried powders are reported in Table 2. The synthesis allowed a good control over the chemical composition of both HAp and Mg-HAp powders, the Ca/P and (Ca + Mg)/P atomic ratios being close to the stoichiometric value of 1.667. Only in the case of sample 1.0Mg-HAp the (Ca + Mg)/P molar ratio showed a strong deviation from the nominal composition, the value being 1.518. Thus, the increased Mg content led to a calcium-deficient phase whose (Ca + Mg)/P molar ratio was very close to that of TCP (Ca/P 1.500).

Particle size and morphology of as-dried powders were determined by TEM observations. In Fig. 1 TEM images and SAED (selected area electron diffraction) patterns of all samples are presented. It resulted that samples are composed of needle-like nanoparticles of length 50–100 nm and width 10–20 nm. SAED patterns exhibit spotted sharp and continuous rings that evidence polycrystalline grains.

TG curves of all as-dried precipitates showed weight losses between 3% and 5% in the range 150–600 °C, associated to the loss of combined water and carbonates, based on previous experimental data[7] and as also stated by the FTIR analyses below.

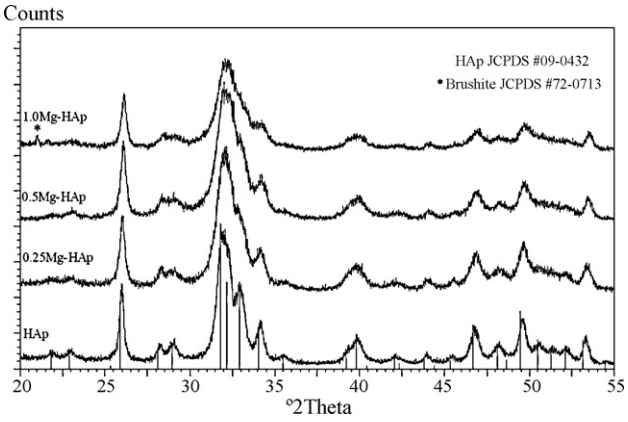

Fig. 2. XRD patterns of as-dried HAp, 0.25Mg-HAp, 0.5Mg-HAp and 1.0Mg-HAp nanopowders.

XRD patterns of as-dried pure and magnesium substituted hydroxyapatite powders are compared in Fig. 2. All XRD spectra showed reflections associated to either HAp [JCPDS #09-0432] and amorphous calcium phosphate (ACP).[1] The broad band typical of ACP were more evident in the case of Mg-HAp samples, especially in the 2θ range between 28° and 32° and between 45° and 55°.[1,17–19] These observations were supported by the results on the crystallinity degree. In fact, the estimated value

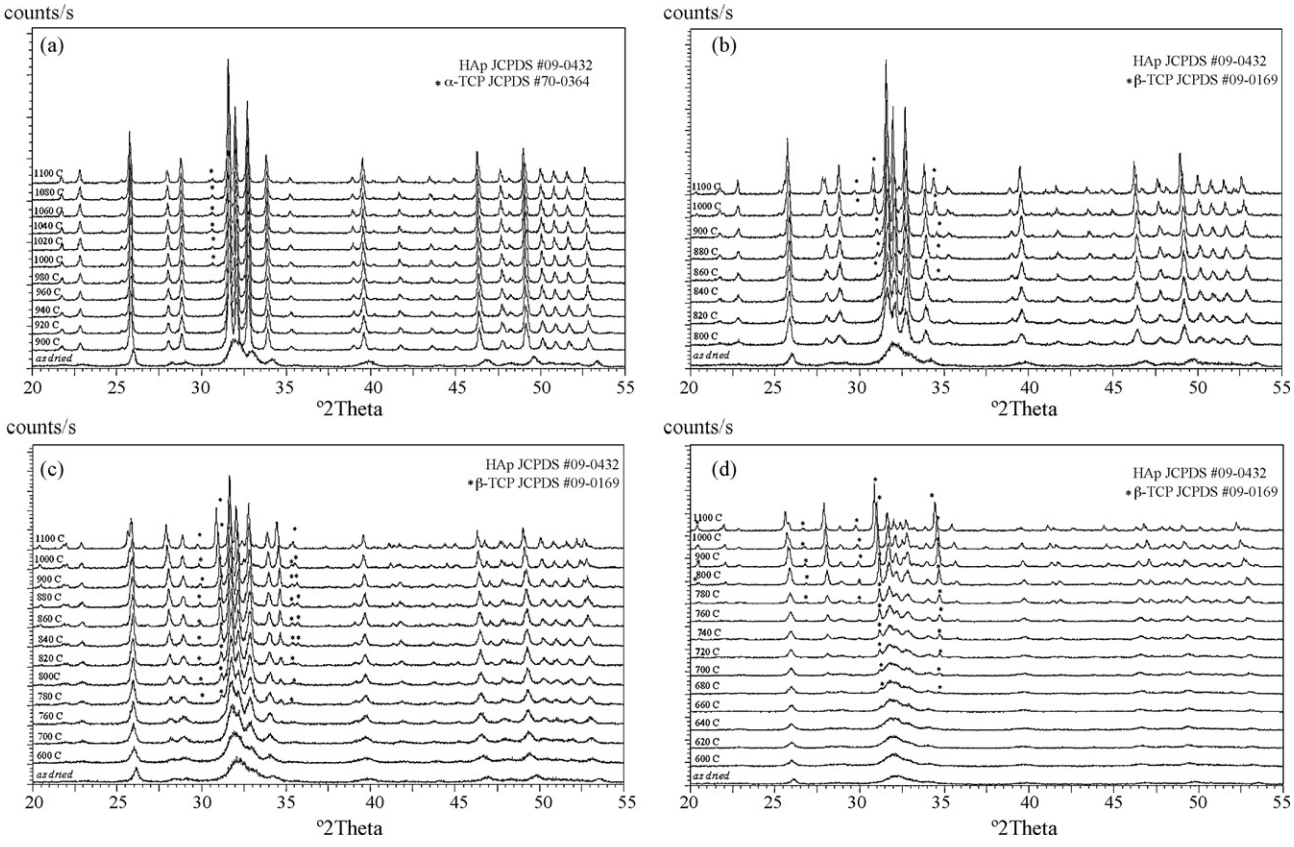

Fig. 3. (a) HT-XRD spectra of sample HAp recorded between 30 and 1100 °C. (b) HT-XRD spectra of sample 0.25Mg-HAp recorded between 30 and 1100 °C. (c) HT-XRD spectra of sample 0.5Mg-HAp recorded between 30 and 1100 °C. (d) HT-XRD spectra of sample 1.0Mg-HAp recorded between 30 and 1100 °C.

was about 60% for the pure HAp, and 48%, 40% and 30%, for 0.25Mg-HAp, 0.5Mg-HAp, and 1.0Mg-HAp, respectively. Thus in good agreement with the literature,[4,20,21] the crystallinity degree progressively decreased with increasing the Mg content.

The mean crystallite size of as-dried HAp sample was about 44 nm and about 11 nm, along *c* and *a* axis, respectively. In the case of Mg-HAps it was 31, 23, and 30 nm along *c* axis and 10, 11, and 12 nm along the *a* axis, for 0.25Mg-HAp, 0.5Mg-HAp, and 1.0Mg-HAp, respectively.

3.2. Thermal stability and thermal behaviour of pure and Mg-substituted hydroxyapatites

In order to follow the phase evolution of the powders and to accurately define the thermal decomposition temperature, HT-XRD analyses were performed and the patterns of samples HAp and Mg-HAps are collected in Fig. 3a–d.

It has been evidenced that pure HAp decomposed above 960 °C. The thermal stability of Mg-substituted hydroxyapatites showed a distinct decreasing trend with increasing the Mg content. In particular, 0.25Mg-HAp was thermally stable up to 840 °C, 0.5Mg-HAp up to 760 °C and 1.0Mg-HAp up to 660 °C.

According to the literature,[22] the incorporation of Mg^{2+} led to a gradual transformation of HAp in *whitlockite* between 300 and 1000 °C, depending on the actual magnesium content. The temperature onset of the thermal decomposition decreased while increasing the Mg content.[4] The destabilizing effect of Mg is imputable to the smaller ionic radius of Mg^{2+} (0.65 Å) with respect to Ca^{2+} (0.99 Å).[22]

Calculated cell parameters and volume fraction of β-TCP (X_β) are presented in Table 3a, obtained on the spectra of pure and substituted HAps after calcination at 1100 °C. In good agreement with the literature,[17,20,21,23,24] a slight contraction of lattice parameters was detected, due to the smaller ionic radius of Mg^{2+}. Only in the case of 1.0Mg-HAp, an increment of lattice parameter *a* was detected.

In Table 3b, 2θ and *d*-spacing values of (0 2 1 0) plane relative to the above β-TCP phase are compared with data reported in the JCPDS cards of β-TCP (*JCPDS #09-0169*) and of 1.50 wt% Mg-substituted TCP ($Ca_{2.81}Mg_{0.19}(PO_4)_2$, (*JCPDS #70-0682*).

It can be observed that in the case of HAp sample the 2θ and *d*-spacing values were very close to those reported in *JCPDS #09-0169* for β-TCP. On the other side, the values derived from the XRD patterns of Mg-HAp samples showed a considerable shift with respect to *JCPDS #09-0169*, resulting much closer to those of *JCPDS #70-0682*. These results were in good agreement with the literature data and further support the stabilisation of β-TCP by Mg substitution.[22]

Table 3a
Calculated cell parameters of pure and Mg-substituted hydroxyapatite powders.

Sample	*a* [Å]	*b* [Å]	*c* [Å]	*V* [10^6 pm^3]	X_β (%v)
HAp	9.422(3)	9.422(3)	6.881(3)	528.519	8
0.25Mg-HAp	9.416(2)	9.416(2)	6.879(1)	528.209	12
0.5Mg-HAp	9.419(6)	9.419(6)	6.879(4)	528.500	21
1.0Mg-HAp	9.44(1)	9.44(1)	6.866(7)	529.630	80

Table 3b
Diffraction angles (2θ) and *d*-spacings derived from experimental XRD patterns of HAp and Mg-HAps samples calcined at 1100 °C and comparison with selected JCPDS.

Sample	(0 2 1 0) Plane	
	d-spacing (Å)	2θ
HAp	2.8778	31.051
0.25Mg-HAp	2.8529	31.329
0.5Mg-HAp	2.8548	31.308
1.0Mg-HAp	2.8483	31.381
JCPDS #09-0169 (β-$Ca_3(PO_4)_2$)	2.8800	31.026
JCPDS # 70-0682 ($Ca_{2.81}Mg_{0.19}(PO_4)_2$)	2.8549	31.306

According to Ryu et al.[25] these results suggest that Mg is preferentially incorporated into the β-TCP phase, the replacement of Ca by Mg inducing a lattice contraction and the respective displacement toward higher 2θ angles of the β-TCP reflections. The effect of the Mg incorporation becomes more and more evident as the Mg content increases.[4,25,26]

In order to investigate the effect of the presence of magnesium on the β → α-TCP phase transition, Mg-HAp samples were calcined in the range 1300–1500 °C for 2 h and XRD analysis was performed (Fig. 4). According to the literature,[1] in pure HAp the β → α-TCP transition usually occurred above 1100 °C. In the case of Mg-HAp samples, the α-TCP phase appeared only above 1300 °C, due to the stabilization of the β-TCP polymorph associated with magnesium incorporation,[6] improving the HT-XRD results previously discussed.

Concluding, it resulted that Mg-substituted HAps synthesised by wet methods were less thermally stable than the pure HAp, the presence of Mg^{2+} ions increasing the stability of the ACP phase against the conversion into apatite.[2] The literature statements were confirmed since Mg-substituted ACP converted into HAp and/or *whitlockite*, depending on composition. The incorporation of Mg in the apatite lattice resulted in a further stabilization of the β-TCP polymorph.

Moreover, thermal analyses (DTA) were also performed in order to further investigate this point.

As previously assessed, pure HAp sample showed only one peak around 1490 °C associated to the allotropic transformation

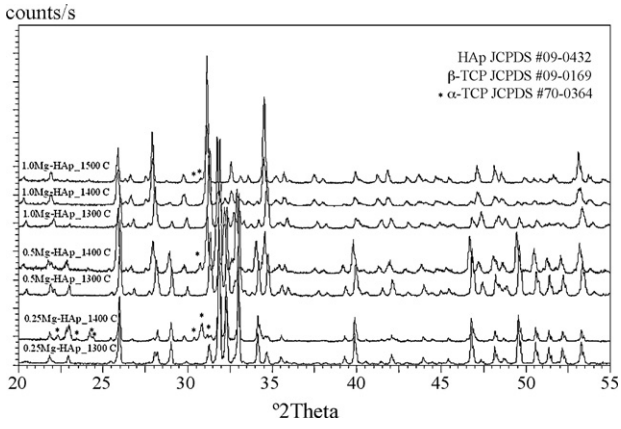

Fig. 4. XRD spectra of 0.25Mg-HAp, 0.5Mg-HAp powders calcined at 1300 °C or 1400 °C, and 1.0Mg-HAp powder calcined at 1300 °C, 1400 °C or 1500 °C.

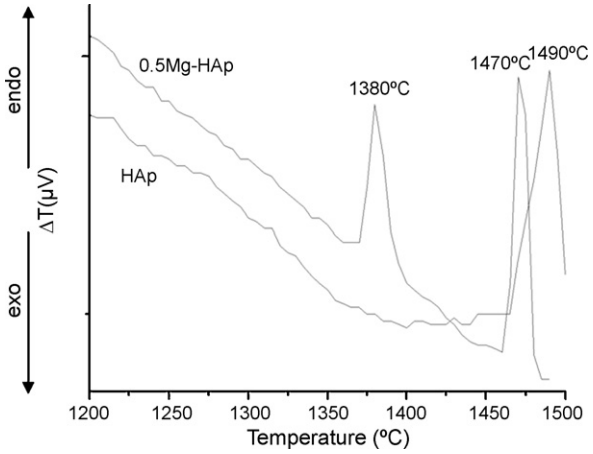

Fig. 5. DTA curves of pure and 0.5Mg-HAp powders.

α-TCP → α′-TCP.[9] In the case of Mg-HAps, all DTA patterns presented similar features: one peak was detected around 1380 °C, due to the β-TCP → α-TCP allotropic transformation, and another one around 1470 °C, related to the high temperature transformation α-TCP → α′-TCP[27] (Fig. 5). Usually, the β-polymorph of TCP is the stable phase up to 1125 °C, at higher temperature the transition to the α-polymorph occurs.[1] In the case of the Mg-HAps, the incorporation of Mg in the apatite lattice result in a stabilization of the β-TCP polymorph at higher temperatures.[2,6]

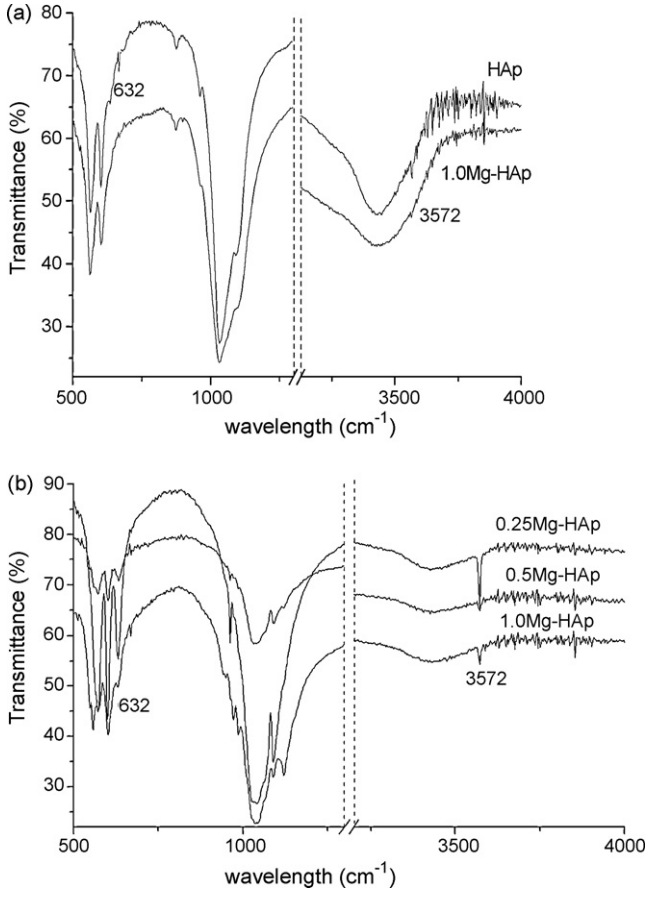

Fig. 6. (a) FT-IR spectra of HAp and 1.0Mg-HAp as-dried powders. (b) FT-IR spectra of 0.25Mg-HAp, 0.5Mg-HAp and 1.0Mg-HAp calcined at 1100 °C.

3.3. FT-IR study of pure and Mg-substituted hydroxyapatites

The FT-IR spectra of as-dried samples are reported in Fig. 6a, patterns of samples calcined at 1100 °C are compared in Fig. 6b. The FT-IR spectra of as-dried samples present the characteristic pattern of partially carbonated hydrated hydroxyapatites, as extensively discussed elsewhere[7]: strong bands in the range 1460–1410 cm^{-1} indicating that carbonate groups substitute PO_4^{3-} in the hydroxyapatite lattice[13,28] and further, bands at 3570 and 631 cm^{-1}, corresponding to the stretching and vibrational mode of the OH^- groups, respectively (Fig. 6a). Moreover, according to the literature, Mg-HAps showed a decreased intensity of OH^- vibration modes at 630 and 3570 cm^{-1}, as well as a broadening of PO_4^{3-} bands with respect to HAp sample (Fig. 6a), the effect increased with the Mg content.[4,20] These effects are typical for Mg-substituted hydroxyapatites synthesized by wet methods and can be explained by the increased lattice disorder due to HPO_4^{2-} substitutions, the latter usually increased with the Mg content.[2,4,17,26]

Table 4
Specific surface area (SSA) and average particle size (D_{BET}) of pure and Mg-substituted hydroxyapatite powders.

Sample	As-dried[a] (m^2/g)	Calcined at 600 °C (m^2/g)	D_{BET}[b] (nm)
HAp	77	45	25
0.25Mg-HAp	51	32	37
0.5Mg-HAp	142	68	13
1.0Mg-HAp	87	27	22

[a] Samples were preliminarily treated with EtOH in order to eliminate absorbed water.
[b] The average particle size (D_{BET}) was calculated on as-dried sample.

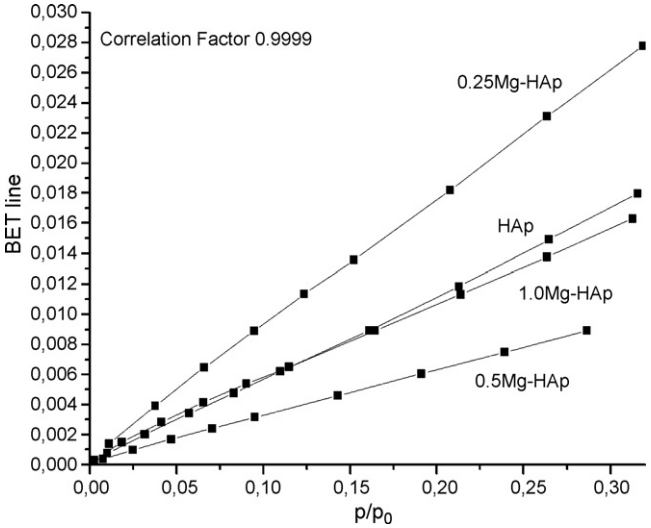

Fig. 7. BET lines of as-dried samples of pure and Mg-substituted hydroxyapatites.

However, it is generally difficult to distinguish between HPO_4^{2-} and CO_3^{2-} groups due to the overlapping of the characteristic peaks around 870 cm^{-1}.[2] FT-IR of calcined samples differ considerably from as-dried materials (Fig. 6b). In details, all bands associated to carbonate ions disappeared, bands associated to combined water at 1636 and 3430 cm^{-1} decreased sensibly, only for HAp sample the intensity of OH vibration modes at 632 and 3572 cm^{-1} increased sensibly. For all Mg-HAps, it was evidenced that the intensity of these peaks decreased with increasing the Mg content (Fig. 6b). Moreover, as the Mg content increased, a slight shift of the OH^- peak at 3572 cm^{-1} and a considerable broadening of the 700–1700 cm^{-1} phosphate bands were observed.[29]

In detail, in the case of 1.0Mg-HAp sample, extra peaks at 942, 948, 962, 972, 986[1], 1044, 1090, 1120 cm^{-1} were detected. These bands can be ascribed to the PO_4^{3-} vibration modes characteristic of tricalcium phosphate, in good agreement with Pena and Vallet-Regi[30] (Fig. 6b). In fact a high content of β-TCP

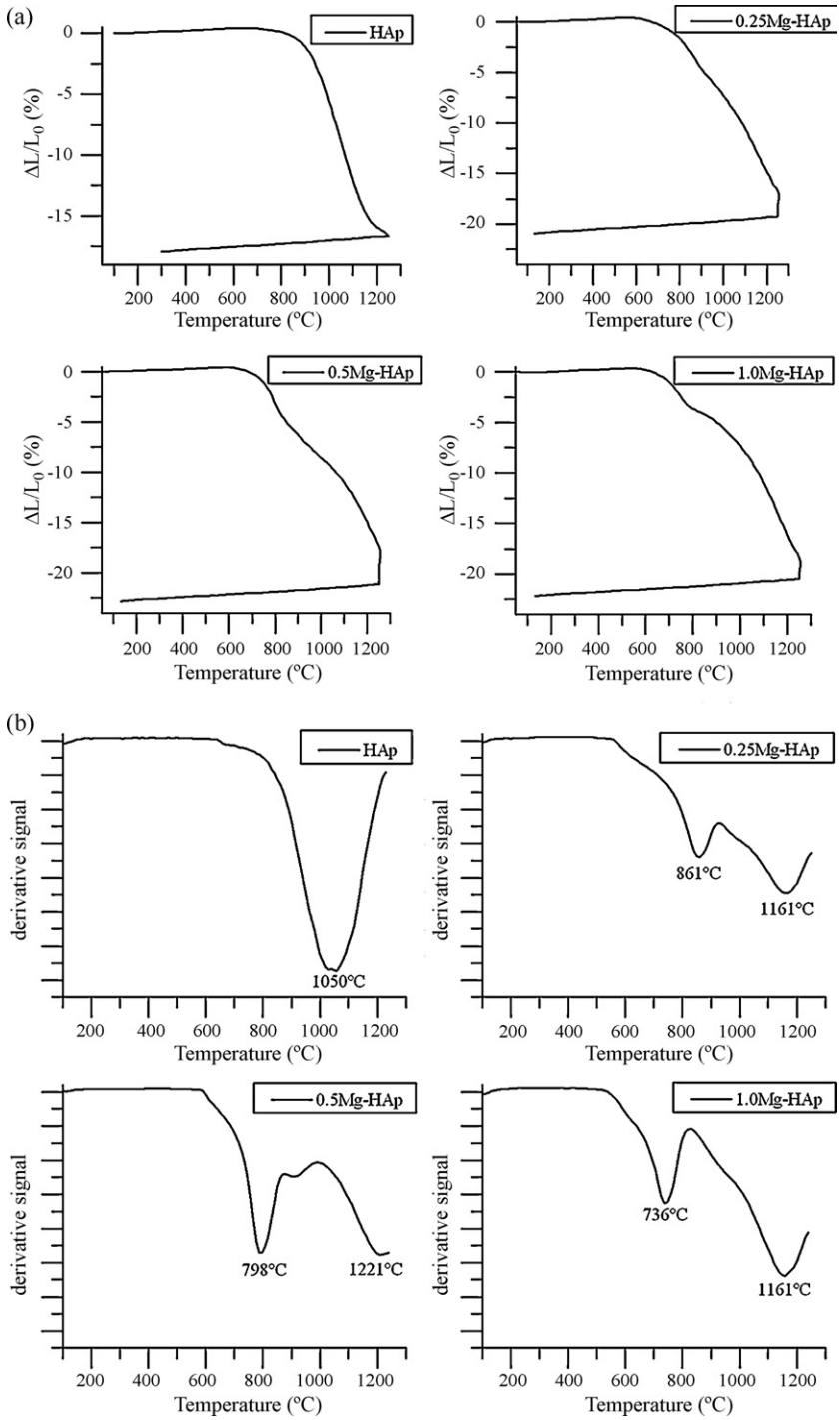

Fig. 8. (a) Dilatometric curves of pure HAp, 0.25Mg-HAp, 0.5Mg-HAp and 1.0Mg-HAp. (b) Derivative curves of pure HAp, 0.25Mg-HAp, 0.5Mg-HAp and 1.0Mg-HAp.

Table 5
Density and sintering data of pure and Mg-substituted hydroxyapatite materials.

Sample	Green density (g/cm^3) [%][a]	Fired density (g/cm^3) [%] 1250 °C[a]	Linear shrinkage (%)	Inflection temperature (°C)
HAp	1.68 [53]	2.90 [92]	18	1040
0.25Mg-HAp	1.49 [47]	2.69 [85]	21	861–1161
0.5Mg-HAp	1.44 [46]	2.68 [85]	23	798–1221
1.0Mg-HAp	1.43 [45]	2.68 [85]	22	736–1161

[a] Theoretical value of pure HAp, $d_{th} = 3.156$ g/cm^3.

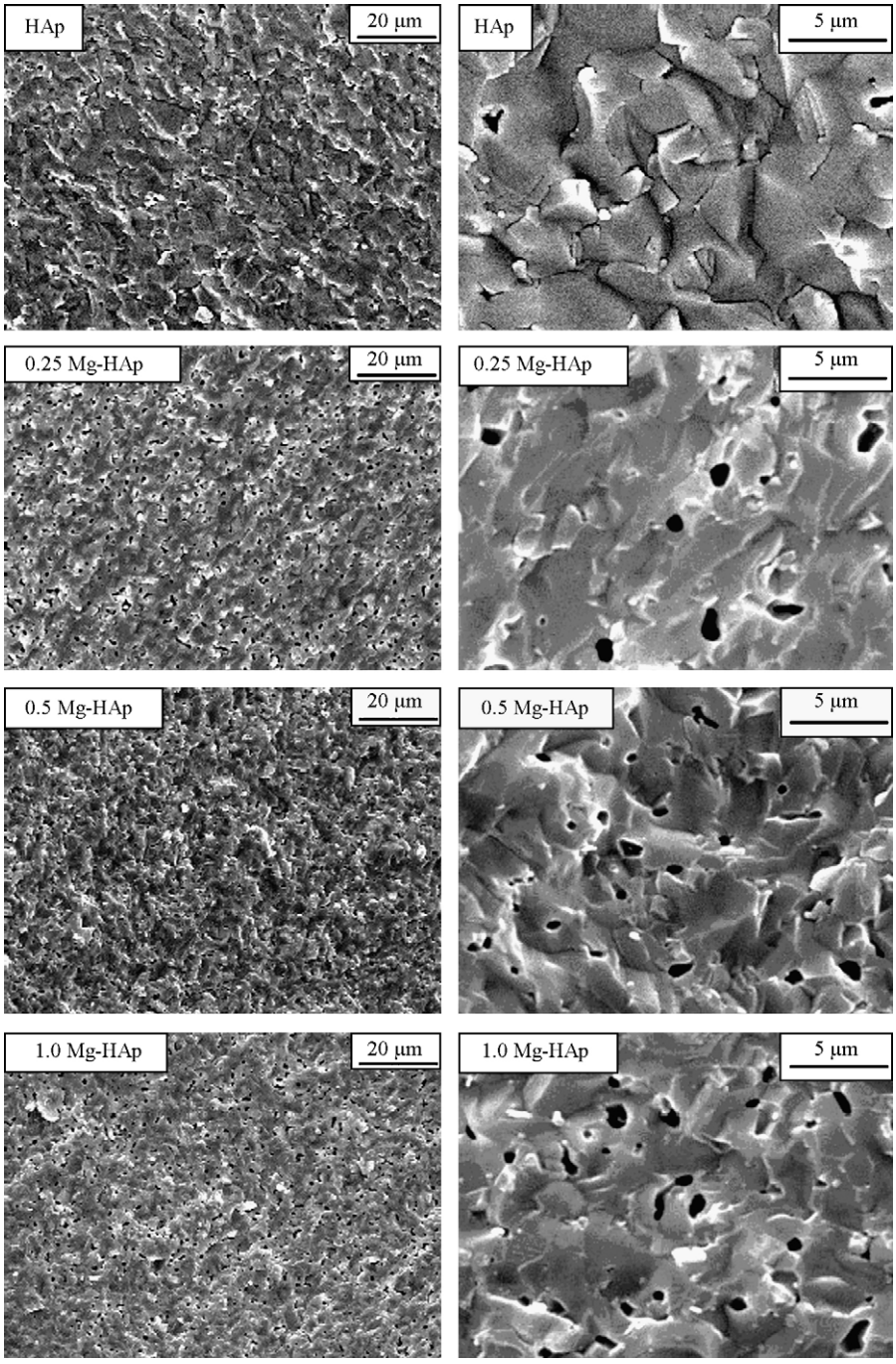

Fig. 9. SEM micrographs of fracture surfaces of pure and Mg-substituted hydroxyapatites.

is present as second phase in 1.0Mg-HAp powder calcined at 1100 °C (Table 3a), as shown in high temperature X-ray diffraction pattern (Fig. 3d).

3.4. Specific surface area of pure and Mg-substituted hydroxyapatites

The average particle size (D_{BET}) of as-dried nanopowders as well as the specific surface area (SSA) of as-dried and 600 °C-calcined powders are presented in Table 4. In Fig. 7 the BET plots of all as-dried samples are reported. Sample 0.5Mg-HAp showed the highest SSA, and, as expected, calcination induced a lowering of SSA values, particularly for the 1.0Mg-HAp. The calculated D_{BET} ranged between 13 and 37 nm. The results were in agreement with TEM observations (Fig. 1) and the mean crystallite size as determined by XRD.

It can be observed that in the case of 0.25Mg-HAp and 0.5Mg-HAp nanopowders, the particle size decreased with Mg content, in good agreement with Zyman et al.[29] As reported in Table 2, both as-dried samples showed a (Ca + Mg)/P ratio close to the stoichiometric value of HAp (i.e. 1.667) and presented a low volume fraction of β-TCP (Table 3a). On the other side, sample 1.0Mg-HAp was characterized by a (Ca + Mg)/P ratio close to that of TCP (i.e. 1.500) and contained a much higher volume fraction of β-TCP (Table 3a). As a consequence, the average particle size of this sample did not follow the expected trend.[29]

3.5. Sintering behaviour of pure and Mg-substituted hydroxyapatites

The dilatometric curves and the linear shrinkage rate of the different samples are compared in Fig. 8a and b, up to 1250 °C.

Pure HAp showed an onset shrinkage temperature around 740 °C, the maximum sintering rate temperature being located at about 1050 °C. The shrinkage was completely recovered during the heating step and reached a total value of about 18%.

On the other side, Mg-substituted HAps presented an onset temperature at approximately 680 °C for the lower magnesium substituted powders, while at 630 °C in the case of 1.0Mg-HAp; the related shrinkage can be reasonably associated to the beginning of the phase decomposition,[17] which then overlapped to the starting densification. This phenomenon also implies the appearance of the first peak on the derivative curves, centred at 861, 798 and 736 °C for $x = 0.25$, 0.5 and 1.0, respectively. In the case of samples 0.25Mg-HAp and 0.5Mg-HAp, these results were in good agreement with HT-XRD analyses. On the other side, for sample 1.0Mg-HAp, containing an higher Mg amount, the decomposition temperature determined by means of HT-XRD measurements was lower, *e.g.* 660 °C.

Furthermore, the maximum sintering rate temperatures of Mg-HAp materials are displaced to higher values with respect to pure HAp, and a higher total shrinkage was recovered, probably associated to the incorporation of the smaller Mg^{2+} ions on Ca(V) sites in the TCP lattice with a consequent β-stabilization.[14] In fact, the maximum shrinkage rate temperature, from the second peak on the derivative curves, was placed at 1161 °C for 0.25Mg-HAp and 1.0Mg-HAp and at 1221 °C for 0.5Mg-HAp, the total shrinkage being 21%, 23% and 22% for 0.25Mg-HAp, 0.5Mg-HAp and 1.0Mg-HAp, respectively. A part of this shrinkage was recovered during the isothermal step, so that dilatometric analyses at lower temperatures were not performed.

Green and fired densities are collected in Table 5. The comment to these data is difficult to be performed since all the materials presented variable amounts of second phases, precisely α-TCP and β-TCP for pure and Mg-HAps, respectively, having a different theoretical density than pure HAp. A more precise comparison on the final densification achieved by the different materials can be performed exploiting the SEM micrographs of the materials sintered at 1250 °C for 1 h (Fig. 9).

The final densities of Mg-substituted HAps are lower than HAp one, in good agreement with literature data[31]; this is due to a more relevant residual porosity, whose amount seems to increase with the Mg content. The pores, having a diameter of about 0.8–1.0 μm, are surrounded by a ceramic matrix characterized by a relevant grain coalescence, as in the case of the pure HAp.

4. Conclusions

High specific surface area Mg-substituted hydroxyapatite nanopowders ($Ca_{10-x}Mg_x(PO_4)_6(OH)_2$, $x = 0.25$,0.5 and 1.0) were successfully pursued by precipitation, starting from $Ca(NO_3)_2{\cdot}4H_2O$, $(NH_4)_2HPO_4$ and $Mg(NO_3)_2$. Up to $x = 0.5$, the process allowed a good control of the chemical composition of Mg-substituted hydroxyapatite nanocrystals. The further increase of Mg content induced the formation of a calcium deficient phase. The crystallinity degree of as-dried precipitates decreased with increasing the Mg content. A slight decrement of the lattice parameters was observed up to $x = 0.5$. The volumic fraction of TCP increased with Mg content accompanied by decreased thermal decomposition temperature. The incorporation of Mg promoted the formation of the β-TCP phase and resulted in the stabilization of the β-polymorph up to 1300–1400 °C.

All materials showed good sinterability, the maximum sintering rate temperatures of Mg-HAp materials were displaced to higher values with respect to pure HAp. The Mg incorporation induced an increased residual porosity (i.e. average pore size about 1 μm).

Acknowledgments

This work was supported by PRIN 2006-2008 project titled "Design and realization of organic, inorganic and hybrid nanostructured scaffolds as substrates for the differentiation of stem cells in regenerative medicine"

The authors wish to acknowledge Dr. C. Bellitto and Dr. E. Bauer, ISM, CNR-Montelibretti, Rome-Italy, for FT-IR facilities and Prof. E. Bemporad and D. De Felicis (University of Rome 3, Rome, Italy) for TEM analyses.

References

1. Elliott, J. C., *Structure and Chemistry of the Apatites and Other Calcium Orthophosphates*. Elsevier Science, Amsterdam, 1994, p. 74.

2. LeGeros, R. Z., *Calcium Phosphates in Oral Biology and Medicine. Monographs in Oral Sciences*. KargerBasel, Switzerland, Basel, 1991, p. 108.
3. Lilley, K., Gbureck, U., Knowles, J., Farrar, D. and Barralet, J., Cement from magnesium substituted hydroxyapatite. *J. Mater. Sci.: Mater. Med.*, 2005, **16**, 455–460.
4. Suchanek, W. L., Byrappa, K., Shuk, P., Riman, R. E., Janas, V. F. and TenHuisen, K. S., Preparation of magnesium-substituted hydroxyapatite powders by the mechanochemical–hydrothermal method. *Biomaterials*, 2004, **25**, 4647–4657.
5. Percival, M., Bone health & osteoporosis. *Appl. Nutr. Sci. Rep.*, 1999, **5**(4), 1.
6. Kim, S. R., Lee, J. H., Kim, Y. T., Riu, D. H., Jung, S. J., Lee, Y. J. *et al.*, Synthesis of Si, Mg substituted hydroxyapatites and their sintering behaviours. *Biomaterials*, 2003, **24**, 1389–1398.
7. Bianco, A., Cacciotti, I., Lombardi, M., Montanaro, L. and Gusmano, G., Thermal stability and sintering behaviour of hydroxyapatite nanopowders. *J. Thermal. Anal. Calor.*, 2007, **88**, 237–243.
8. Clausen, L. and Fabricius, I., BET measurements: outgassing of minerals. *J. Coll. Interf. Sci.*, 2000, **227**, 7–15.
9. Bianco, A., Cacciotti, I., Lombardi, M. and Montanaro, Si-substituted hydroxyapatite nanopowders: synthesis, thermal stability and sinterability. *Mater. Res. Bull.*, 2009, **44**, 345–354.
10. Ayed, F. B., Bouaziz, J. and Bouzouita, K., Calcination and sintering of fluorapatite under argon atmosphere. *J. Alloys Compd.*, 2001, **322**, 238–245.
11. Landi, E., Tampieri, A., Celotti, G. and Sprio, S., Densification behaviour and mechanisms of synthetic hydroxyapatites. *J. Eur. Ceram. Soc.*, 2000, **20**, 2377–2387.
12. Bouyere, E., Gitzhofer, F. and Boulos, M. I., Morphological study of hydroxyapatite nanocrystal suspension. *J. Mater. Sci.: Mater. Med.*, 2000, **11**, 523–531.
13. Tang, X. L., Xiao, X. F. and Liu, R. F., Structural characterization of silicon-substituted hydroxyapatite synthesized by a hydrothermal method. *Mater. Lett.*, 2005, **59**, 3841–3846.
14. Siddharthan, A., Seshadri, S. K. and Sampath Kumar, T. S., Microwave accelerated synthesis of nanosized calcium deficient hydroxyapatite. *J. Mater. Sci.: Mater. Med.*, 2004, **15**, 1279–1284.
15. Sung, Y.-M., Lee, J.-C. and Yang, J.-W., Crystallization and sintering characteristics of chemically precipitated hydroxyapatite nanopowders. *J. Crystal Growth*, 2004, **262**, 467–472.
16. Sung, Y. M. and Kim, D. H., Crystallization characteristics of yttria-stabilized zirconia/hydroxyapatite composite nanopowder. *J. Crystal Growth*, 2003, **254**(7), 411–417.
17. Kannan, S., Lemos, I. A. F., Rocha, J. H. G. and Ferreira, J. M. F., Synthesis and characterization of magnesium substituted biphasic mixtures of controlled hydroxyapatite/β-tricalcium phosphate ratios. *J. Solid State Chem.*, 2005, **178**, 3190–3196.
18. Bertoni, E., Bigi, A., Cojazzi, G., Gandolfi, M., Panzavolta, S. and Roveri, N., Nanocrystals of magnesium and fluoride substitued hydroxyapatite. *J. Inorg. Biochem.*, 1998, **72**, 29–35.
19. Gibson, I. R. and Bonfield, W., Preparation and characterization of magnesium/carbonate co-substituted hydroxyapatites. *J. Mater. Sci.: Mater. Med.*, 2002, **13**, 685–693.
20. Bigi, A., Falini, G., Foresti, E., Gazzano, M., Ripamonti, A. and Roveri, N., Magnesium influence on hydroxyapatite crystallization. *J. Inorg. Biochem.*, 1993, **49**, 69–78.
21. Bigi, A., Falini, G., Foresti, E. and Ripamonti, A., Rietveld structure refinement of synthetic magnesium substituted β-tricalcium phosphate. *Zeitschrift fur Kristallographic*, 1996, **211**, 13–16.
22. Fadeev, I. V., Shvorneva, L. I., Barinov, S. M. and Orlovskii, V. P., Synthesis and structure of magnesium-substituted hydroxyapatite. *Inorg. Mater.*, 2003, **39**(9), 947–950.
23. Mayer, I., Schlam, R. and Featherstone, J. D. B., Magnesium containing-carbonate apatites. *J. Inorg. Biochem.*, 1997, **66**(1), 1–6.
24. Yasukawa, A., Guchi, S., Kandori, K. and Ishikawa, T., Preparation and characterization of magnesium–calcium hydroxyapatites. *J. Mater. Chem.*, 1996, **6**, 1401–1405.
25. Ryu, H. S., Hong, K. S., Leb, J. K., Kim, D. J., Lee, J. H., Chang, B. S. *et al.*, Magnesia-doped HA/β-TCP ceramics and evaluation of their biocompatibility. *Biomaterials*, 2004, **25**, 393–401.
26. Suchanek, W. L., Byrappa, K., Shuk, P., Riman, R. E., Janas, V. F. and TenHuisenb, K. S., Mechanochemical–hydrothermal synthesis of calcium phosphate powders with coupled magnesium and carbonate substitution. *J. Solid State Chem.*, 2004, **177**, 793–799.
27. Descamps, M., Hornez, J. C. and Leriche, A., Effects of powder stoichiometry on the sintering of β-tricalcium phosphate. *J. Eur. Ceram. Soc.*, 2007, **27**, 2401–2406.
28. Arcos, D., Rodriguez Carvajal, J. and Vallet-Regi, M., Silicon incorporation in hydroxylapatite obtained by controlled crystallization. *Chem. Mater.*, 2004, **16**, 2300–2308.
29. Zyman, Z., Tkachenko, M., Epple, M., Polyakov, M. and Naboka, M., Magnesium-substituted hydroxyapatite ceramics. *Mat. -wiss. u. Werkstofftech.*, 2006, **37**(6), 474–477.
30. Pena, J. and Vallet-Regi, M., Hydroxyapatite, tricalcium phosphate and biphasic materials prepared by a liquid mix technique. *J. Eur. Ceram. Soc.*, 2003, **23**, 1687–1696.
31. Kalita, S. J. and Bhatt, H. A., Nanocrystalline hydroxyapatite doped with magnesium and zinc: synthesis and characterization. *Mater. Sci. Eng. C*, 2007, **27**, 837–848.